does not show any manifestation of ion-pair formation in terms of an observable g shift. This can be rationalized by considering the orbital symmetries of the cation and anion and the possible structures of the ion pair. The highest occupied molecular orbital (HOMO) of TMB, from which one electron is removed to form $TMB^{+}\cdot$, has a nodal plane passing through carbons 3 and 6 (Figure 4a). If the ion pair with I^- has a structure in which the counteranion is placed on the yz nodal plane (such as Figure 4a) or in which the anion vibrates symmetrically with respect to this plane, there will be no net overlap between the p orbitals on I^- and the π orbital of $TMB^{+}\cdot$ and hence no observable g shift. If the ion pair were to have a structure in which the anion is located away from the yz plane (for example, Figure 4b) an appreciable overlap between the HOMO of $TMB^{+}\cdot$ and appropriate p orbitals on I^- could produce an observable g shift. The lack of an experimentally observed g shift is therefore consistent with ion-pair formation between $TMB^{+}\cdot$ and I^- if the structure of the ion pair is similar to Figure 4a.

If the $TMB^{+}\cdot$ and I_3^- ion pair were to have a structure analogous to the $TMB^{+}\cdot$ I^- ion pair (i.e., Figure 4c),[33] the observed g shift could be explained. Overlap between the nonbonding p orbitals of the terminal iodine atoms of appropriate symmetry with the HOMO of $TMB^{+}\cdot$ could result in a net transfer of electron density from I_3^- to $TMB^{+}\cdot$. Thus the excited-state TMB $I_3\cdot$ would mix with the ground-state $TMB^{+}\cdot$ I_3^- resulting in a large g shift.

The similar interactions noted for 1,4-$DMA^{+}\cdot$ and $PTH^{+}\cdot$ with I_3^- and the lack of interaction observed for $TMTH^{+}\cdot$ and 9,10-$DMA^{+}\cdot$ may also be related to the structure of the ion pairs. Further work on the effect of ion-pair structure on the magnitude of the g shift and on the effect of solvent on the equilibrium constant are currently underway.

Acknowledgment. This investigation was supported by Grant CHE-76-04166 from the National Science Foundation.

References and Notes

(1) F. C. Adam and S. I. Weissman, *J. Am. Chem. Soc.*, **80**, 1518 (1958).
(2) N. W. Atherton and S. I. Weissman, *J. Am. Chem. Soc.*, **83**, 1330 (1961).
(3) N. Hirota, *J. Phys. Chem.*, **71**, 127 (1967).
(4) A. M. Herman, A. Rembaum, and W. R. Carper, *J. Phys. Chem.*, **71**, 2661 (1967).
(5) G. R. Stevenson and A. E. Alegria, *J. Phys. Chem.*, **78**, 1771 (1974).
(6) G. R. Stevenson, R. Concepcion, and I. Ocasio, *J. Phys. Chem.*, **80**, 861 (1976).
(7) G. R. Stevenson and L. Echegoyen, *J. Phys. Chem.*, **77**, 2339 (1973).
(8) G. R. Stevenson and I. Ocasio, *J. Am. Chem. Soc.*, **98**, 980 (1976).
(9) R. D. Allendoerfer and R. J. Papez, *J. Phys. Chem.*, **76**, 1012 (1972).
(10) G. R. Stevenson and A. E. Alegria, *J. Phys. Chem.*, **79**, 1042 (1975).
(11) T. Yonezawa, T. Kawamura, M. Ushio, and Y. Nakao, *Bull. Chem. Soc. Jpn.*, **43**, 1022 (1970).
(12) D. Romans, W. H. Brunlng, and C. J. Michejda, *J. Am. Chem. Soc.*, **91**, 3859 (1969).
(13) S. P. Sorensen and W. H. Bruning, *J. Am. Chem. Soc.*, **95**, 2445 (1973).
(14) J. Fajer, D. C. Borg, A. Forman, R. H. Felton, L. Vegh, and D. Dolphin, *Ann. N.Y. Acad. Sci.*, **206**, 349 (1973).
(15) G. Goez-Morales and P. D. Sullivan, *J. Am. Chem. Soc.*, **96**, 7232 (1974).
(16) A. J. Bard, A. Ledwith, and H. J. Shine, *Adv. Phys. Org. Chem.*, **13**, 155 (1976).
(17) It has been shown that the equilibrium constant for $I_2 + I^- \rightleftarrows I_3^-$ is approximately 10^7 in nitromethane and acetonitrile. [See J. C. Manchon, *C. R. Acad. Sci., Ser. C*, 1123 (1968).]
(18) B. G. Segal and G. K. Fraenkel, *J. Chem. Phys.*, **43**, 4191 (1965).
(19) The observed small shifts in g value measured for $AlCl_3$-oxidized TMB in a variety of solvents[15] are believed to arise from solvent effects[11] rather than from effects of ion pairing.
(20) W. Geogolczyk, S. Slomkowski, and S. Penczek, *J. Chem. Soc., Perkin Trans. 2*, 1729 (1977).
(21) U. Mayer, *Coord. Chem. Rev.*, **21**, 159 (1976).
(22) R. M. Keekra and J. L. Andrews, *J. Am. Chem. Soc.*, **84**, 3635 (1962).
(23) C. P. Wright, D. M. Murray-Rut, and H. Hartley, *J. Chem. Soc.*, 199 (1931).
(24) R. S. Baum and A. I. Popov, *J. Solution Chem.*, **4**, 441 (1975).
(25) A. I. Popov and N. E. Skelly, *J. Am. Chem. Soc.*, **76**, 5309 (1954).
(26) This result is also consistent with a similar extent of dissociation of alkali metal triiodides in CH_3NO_2, although the literature suggests that they are completely dissociated.[25]
(27) P. Walden and E. J. Birr, *Z. Phys. Chem. (Leipzig)*, **163**, 263 (1932).
(28) The possible deprotonation of $PTH^{+}\cdot$ was also considered but it is known that this equilibrium is only important in very basic conditions and that the radical cation is very stable in acetonitrile. [See P. Hansen and R. O. C. Norman, *J. Chem. Soc., Perkin Trans. 2*, 264 (1973).]
(29) S. Hunig, *Pure Appl. Chem.*, **15**, 109 (1967).
(30) O. Hammerich and V. D. Parker, *Electrochim. Acta*, **18**, 537 (1973).
(31) U. Svanholm, O. Hammerich, and V. D. Parker, *J. Am. Chem. Soc.*, **97**, 101 (1975).
(32) It should be noted that in all cases the measured K_d values have not been corrected for ionic strength effects. Since the solutions used were quite dilute ($<10^{-2}$ M) such corrections should be small.
(33) This structure assumes that both $TMB^{+}\cdot$ and I_3^- are planar species. This is substantiated for $TMB^{+}\cdot$ by the magnitude and temperature independence of the methoxyl group proton splitting constants which if they were nonplanar would have greatly reduced splittings and be quite temperature dependent (see P. D. Sullivan, *J. Phys. Chem.*, **74**, 2563 (1970)). The structure of I_3^- is known to be planar (see J. H. Perlstein, *Angew. Chem., Int. Ed. Engl.*, **16**, 519 (1977)).

Tunnelling in Collinear Light–Heavy–Heavy Reactions

Werner Jakubetz

Contribution from the Institut fur Theoretische Chemie und Strahlenchemie der Universitat, A-1090 Wien, Austria. *Received June 14, 1978*

Abstract: For reactions of Mu, H, D, or T with F_2 or Cl_2, mathematically one-dimensional unsymmetric Eckart barrier permeabilities calculated within the vibrationally adiabatic model agree extremely well with exact quantum collinear reaction probabilities using extended LEPS surfaces. The corresponding rate constants and activation energies, in the temperature interval 230–900 K, are also in very good agreement. Other approximations, e.g., the parabolic barrier, have also been tested but are found to be less suitable. In particular, assumption of conservation of vibrational energy leads to considerable errors.

I. Introduction

A large number of investigations of tunnelling effects in chemical reactions (see, e.g., ref 1-4) have employed correction factors relating to mathematically one-dimensional (M1D) potential barriers of the Eckart or Bell type, for which the permeabilities can be given in analytic form.[5-8] Depending on the choice of the underlying basic approach—mostly transition-state theory (TST)[1,2,9,10]—and reaction system—mostly $H + H_2$—there arise some problems that must be considered carefully in assessment of the utility of the tunnelling corrections. Among the points of interest in this respect are the choice of a correct potential surface when comparing with experi-

0002-7863/79/1501-0298$01.00/0

mental results,[4,11] the validity of TST and the separability assumption,[4,12,13] the neglect of reaction path curvature,[14,15] adiabaticity or internal energy conservation (including the definition of the proper effective potentials),[3,16-19] the definition of a proper (tunnelling) reaction path, which may not be identical with the usual minimum energy path ("corner cutting"),[20] errors eventually introduced by the reduction of the dimensionality of tunnelling,[21] and errors due to the inflexibility of the Eckart or Bell potentials, particularly those connected with threshold behavior of the reaction.[3,21,22]

Investigations avoiding a number of these pitfalls have concentrated on collinear reactions, using exact quantum results as reference.[3,11,18,19,21,22] Conclusions drawn from these tests—H + H_2 again—were generally not favorable for the use of Eckart potentials (even less so for the Bell parabola).

Other reactions for which exact collinear quantum reaction probabilities are available, and which might hence serve as additional test examples, include the reactions of various hydrogen isotopes with F_2 or Cl_2.[23-27] Now the specific characteristics of these reactions make it seem probable from the outset that simple tunnelling approaches might work better than for the H + H_2 reaction. Certainly, although in this respect not differing from H + H_2, the energy dependence of the reaction probabilities strongly resembles that of M1D barrier permeabilities. However, in contrast to H + H_2, the barriers of the potential energy surfaces for H + F_2 or Cl_2 are located far out in the reactant valleys. This means that there is no significant reaction path curvature before, near, or at the saddle point (transition state). This feature should result in negligible curvature effects, should facilitate separability of reaction path motion, and will provide little opportunity for corner cutting reaction paths thus making the minimum energy path the most likely tunnelling path. With respect to TST, an equilibrium phase space distribution is very likely to be maintained at the transition state.[28] Since in these cases the transition state can approximately be thought of as a slightly perturbed reactant molecule, the concept of vibrational adiabaticity at the transition state (VA)[3,16,17,29-31] should hold. However, conservation of vibrational energy (CVE)[2,32] would not differ very much from VA and might also be advocated; comparison with the exact results should resolve this problem.

Finally, the potential barriers are far lower for the hydrogen-halogen reactions than for the H + H_2 case. Extreme threshold regions where reaction probabilities are smaller than 0.01 are therefore not expected to contribute significantly to reaction rates in the interesting temperature range around room temperature or above. If the energy range near the top of the barrier dominates in thermal rate constants, then the Eckart potential, being fitted to the exact one at the top of the barrier, ought to be a good approximation.

In this paper the collinear reactions

$$\mathrm{Mu} + \mathrm{F_2}(v) \rightarrow \mathrm{MuF} + \mathrm{F} \quad \text{(R1)}$$

$$\mathrm{H} + \mathrm{F_2}(v) \rightarrow \mathrm{HF} + \mathrm{F} \quad \text{(R2)}$$

$$\mathrm{D} + \mathrm{F_2}(v) \rightarrow \mathrm{DF} + \mathrm{F} \quad \text{(R3)}$$

$$\mathrm{T} + \mathrm{F_2}(v) \rightarrow \mathrm{TF} + \mathrm{F} \quad \text{(R4)}$$

$$\mathrm{Mu} + \mathrm{Cl_2}(v) \rightarrow \mathrm{MuCl} + \mathrm{Cl} \quad \text{(R5)}$$

$$\mathrm{H} + \mathrm{Cl_2}(v) \rightarrow \mathrm{HCl} + \mathrm{Cl} \quad \text{(R6)}$$

$$\mathrm{D} + \mathrm{Cl_2}(v) \rightarrow \mathrm{DCl} + \mathrm{Cl} \quad \text{(R7)}$$

$$\mathrm{T} + \mathrm{Cl_2}(v) \rightarrow \mathrm{TCl} + \mathrm{Cl} \quad \text{(R8)}$$

with the reactant molecules in $v = 0$, 1, and, for (R2) and (R6), in $v = 2$, are treated within the VA approximation using both the Eckart and the Bell approach to represent the M1D potentials along the reaction path. A simple estimate is used to obtain the necessary parameters for the effective potentials from a transition state normal mode analysis. For the $v = 0$ reactant state, the CVE approximation and a hybrid between VA and CVE are also tested. For reactions (R1)-(R4), (R6), and (R7), there exist exact quantum calculations,[23-27] and it will be demonstrated that the quantum reaction probabilities, and hence also the corresponding thermal average rate constants, can be approximated very accurately on the basis of M1D Eckart tunnelling within the framework of the VA theory of collinear reactions.

In section II, the results of the transition state normal mode analysis and the extraction of the effective potential parameters are described. In section III, barrier permeabilities are calculated for the Eckart and Bell potentials, and, where appropriate, are compared with exact quantum reaction probabilities. In the last step, the corresponding thermal rate constants, activation energies, tunnelling corrections, and isotopic rate constant ratios are worked out and again compared with the corresponding quantum results (section IV). Conclusions are in section V.

II. Transition State Properties and Tunnelling Potential Parameters

In the quantum calculations referred to above,[23-27] potential surfaces of the LEPS variety[33] have been used. For reactions (R1)-(R4), the surface number II of Jonathan et al.,[34] with Sato parameters $S_{HF} = 0$ and $S_{FF} = -0.35$, was employed. The surface[35] used by Baer[23] and by Essen et al.[24] in their quantum calculations of reactions (R6) and (R7) has both Sato parameters set to zero. The asymptotic properties of these surfaces have been given before[23,25,34-36] and are not repeated here.

M1D potentials appropriate to describe barrier penetration along the reaction path of the LEPS surfaces are then constructed, using both the asymmetric Eckart function[5] and Bell's inverted parabola.[6,7]

The asymmetric Eckart potential along the reaction coordinate x can be written in terms of exothermicity and barrier height (rather than using the usual[5,8,37] composite parameters)

$$V(x) = QY(x)/\{1 - Y(x)\} - P^2Y(x)/\{1 - Y(x)\}^2 \quad (1)$$

with

$$Y = -\exp(2\pi x/L) \text{ and } P = B^{1/2} + (B + Q)^{1/2}$$

where Q is the exothermicity, B is the barrier height measured from the reactants, and L is a characteristic length related to the tunnelling frequency ν^* and the reduced mass μ for reactant translation,

$$2\pi/L = \pi|\nu^*|(2\mu)^{1/2}P/(B^2 + BQ)^{1/2} \quad (2)$$

Bell's (infinite) inverted parabola is given by

$$V(x) = B - 2\mu\pi^2|\nu^*|^2x^2 \quad (3)$$

and truncation is commonly taken into account by simply ignoring negative energies. Note that ν^* is imaginary and $|\nu^*| = -i\nu^*$. In order to obtain the parameters B, Q, and ν^* necessary to specify the potentials (1) and (3), either in the VA or the CVE approach, a normal mode analysis for the transition state was carried out. The harmonic force constant matrix and the final saddle-point geometry were determined from a simultaneous three-dimensional least-squares fit to the LEPS surface saddle point region of a complete polynomial of the degree three. Using these force constants in Wilson's **FG** formalism,[38] the three harmonic normal mode frequencies $\nu^{\ddagger}_{vib}$, $\nu^{\ddagger}_{\phi}$, and $-i\nu^*_s$ were calculated. The transition state properties for reactions (R1)-(R8) are listed in Table I.

Next, $\nu^{\ddagger}_{vib}$ was inserted into the Morse formula for vibrational energy levels,

Table I. Transition State Properties of LEPS Potential Surfaces

	Mu + F_2[a]	H + F_2[a]	D + F_2[a]	T + F_2[a]	Mu + Cl_2[b]	H + Cl_2[b]	D + Cl_2[b]	T + Cl_2[b]
$r^{\ddagger}_1$/Å[c]			1.897				2.251	
$r^{\ddagger}_2$/Å[d]			1.437				2.017	
$\phi^{\ddagger}$/deg			180				180	
B_s/kJ mol^{-1}			9.84				10.13	
$c^{-1}\nu^{\ddagger}_{vib}$/cm^{-1} [e]	848	787	771	763	546	524	516	512
$c^{-1}\nu^{\ddagger}_{\phi}$/cm^{-1} [e,f]	149	57.8	46.1	41.5	104	37.5	28.3	24.5
$c^{-1}\nu^{*}$/cm^{-1} [e]	1652i	608i	445i	371i	1384i	490i	354i	294i

[a] Surface II of Jonathan et al.[34] [b] Surface of Kuntz et al.[35] [c] Distance X-F or XCl. [d] Distance F-F or Cl-Cl. [e] Masses used: m_{Mu} = 0.114 u, m_H = 1 u, m_D = 2 u, m_T = 3 u, m_F = 19 u, m_{Cl} = 35 u (1 u = 1.6605 × 10^{-24} g). [f] Doubly degenerate.

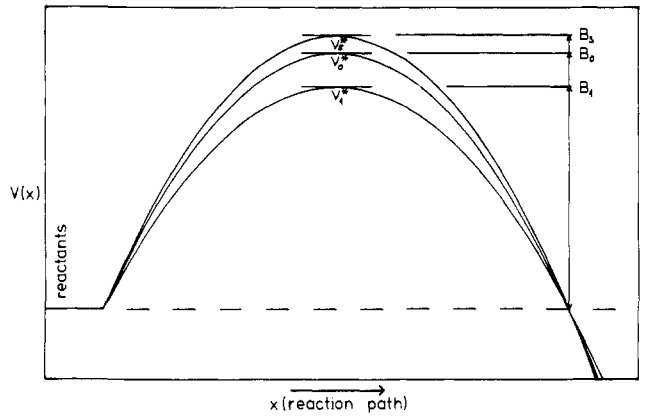

Figure 1. Scaling of tunnelling frequencies ν^* for effective potentials using parabola properties. Drawn to scale for T + F_2.

$$\epsilon_v = \left(v + \frac{1}{2}\right) N_L h\nu - (4D_e)^{-1}\left(v + \frac{1}{2}\right)^2 (N_L h\nu)^2 \quad (4)$$

where D_e is the dissociation energy and N_L is Avogadro's number. The effective VA barrier heights B_v are then determined as the difference between the energy levels ϵ_v at the transition state and the reactant molecule (B_0 is frequently called ΔV^{VAZC}). The CVE barrier height is of course equal to the barrier height of the original potential surface, B_s (the subscript s will henceforth be used to characterize potential surface properties; likewise v, 0, 1, . . . , will refer to effective VA values).

The imaginary frequency ν^*_s describes the shape of the barrier along the reaction path. It is therefore the appropriate value to use for ν^* in the CVE approximation for the M1D potentials (1) and (3). It has also been used frequently, but inconsistently, in a hybrid approach together with the VA barrier height B_0.[21,39] However, Truhlar and Kuppermann[3] have pointed out that a consistent VA theory requires that the tunnelling frequencies of the proper effective potentials be used. In the present paper a simple scaling approximation is used for this purpose. This scaling procedure is depicted schematically in Figure 1. The change in the vibrational frequency of a truncated parabolic barrier on variation of the barrier height, and assuming fixed truncation point and basis width, is described by

$$h\nu^*_v = h\nu^*_s(B_v/B_s)^{1/2} \quad (5)$$

In view of the small differences between B_s and B_0 or B_1 in the present examples, eq 4 will also hold approximately for the true effective potentials. The transition state bending frequencies $\nu^{\ddagger}_{\phi}$ are not required for the collinear case. They have been used in calculations of rate constants for the corresponding three-dimensional rate constants reported in another paper.[40]

Finally, the exothermicities Q have to be specified for the asymmetric Eckart potential (1). Despite the fact that reactions (R1)-(R8) are well known to yield vibrationally excited products,[23-27,34-36] the exothermicities used have been calculated from VA (or CVE) assumptions for the complete reactions. This corresponds to the physical picture that vibrational excitation occurs in a separate step in the curved region of the potential surface, after fully adiabatic barrier transmission. Some sample VA calculations have also been carried out with the exothermicity Q_0 reduced by the product's average vibrational energy content, $Q_0 - \langle E_{v'} \rangle$. Owing to the generally large values of Q, this does not bring about substantial changes in the barrier region of the Eckart potential, and thus in the barrier permeabilities. The use of Q_0 was preferred here as a more generally applicable recipe, since $\langle E_{v'} \rangle$ will normally be unknown for "new" potential surfaces. It should be mentioned that the CVE assumption actually violates zero-point energy requirements for the product molecules; but again using Q_0 instead of Q_s does not lead to any substantial change in the results and therefore the consistent use of the CVE values Q_s was preferred.

The parameter values obtained by the methods outlined above are collected in Table II; values for $v = 2$ which are not included may easily be regenerated from the data given.

III. Reaction Probabilities

The transitional energy (E_T) dependent permeabilities of the M1D barriers (1) and (3) are[5,7,8,37]

$$P^E(E_T) = 1 - \frac{\cosh 2\pi(a-b) + \cosh 2\pi d}{\cosh 2\pi(a+b) + \cosh 2\pi d} \quad (6)$$

and

$$P^B(E_T) = \{1 + \exp 2\pi(B - E_T)/N_L h\nu^*\}^{-1} \quad (7)$$

respectively, where in (6) $a = \frac{1}{2}(E_T/C)^{1/2}$, $b = \frac{1}{2}[(E_T + Q)/C]^{1/2}$, $d = \frac{1}{2}[(P^2 - C)/C]^{1/2}$, and $C = h^2/8\mu L^2$.

Before comparing these permeabilities with collinear quantum reaction probabilities $P_v^Q(E_T)$, it will be useful to discuss briefly the latter. The data for reactions (R1)-(R4) are basically taken from the state path sum calculations of Connor et al.,[25-27] although some additions should be noted. For reaction (R1), the "line of no return" reaction probabilities, which in ref 27 were reported to be somewhat on the low side, have been reanalyzed or recalculated, and extend to higher translational energies, including F_2 ($v = 1$) as well.[41] The revised results are now believed to be accurate to better than ≈3% for the rotated Morse cubic spline fit to the LEPS surface (see below for the further discussion of this point). There are, however, some indications from classical trajectory calculations on this system[43] that the "line of no return" probabilities for Mu + F_2 ($v = 1$) may not tell the whole story, since there may be additional back-reflection from the repulsive wall even at the low translational energies covered here. The "line of no return" probabilities would miss such contributions. No effects like this were observed in trajectory calculations for (R2)-(R4).[43] Results for H + F_2 ($v = 1$) at low values of E_T are a byproduct of the $v = 0$ calculations, but were not reported in

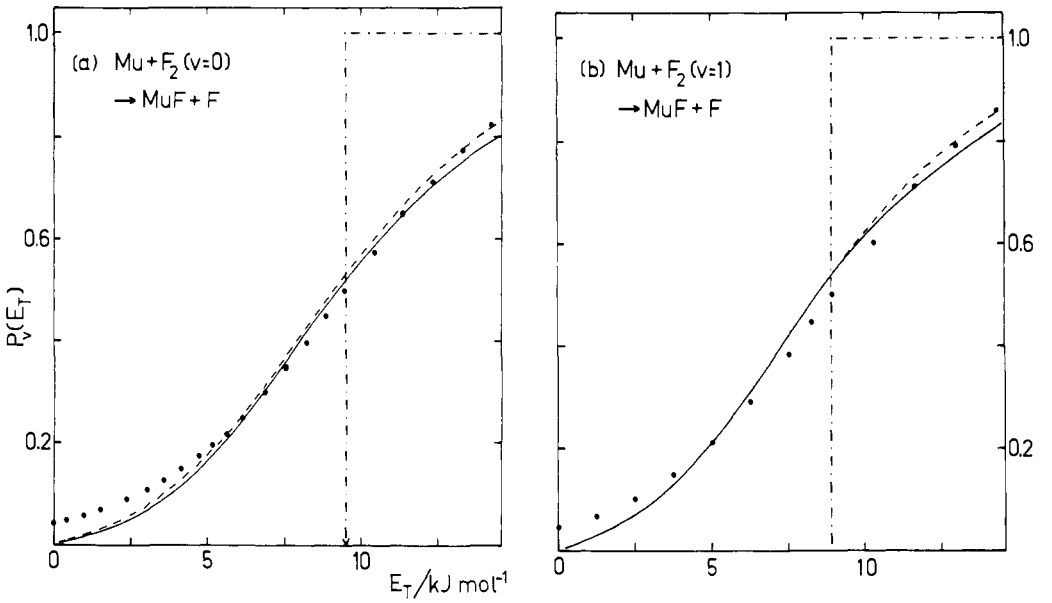

Figure 2. Comparison of quantum reaction probabilities and approximate ones for collinear Mu + F_2 (v). (a) v = 0. (b) v = 1. Full lines (—), quantum calculations;[41] dashed lines (- - -), VA Eckart; filled circles (●), VA Bell; dash-dotted (- ·), VA classical.

Table II. Parameters for Unsymmetric Eckart and Bell Potentials[a,b]

	Mu + F_2	H + F_2	D + F_2	T + F_2	Mu + Cl_2	H + Cl_2	D + Cl_2	T + Cl_2
Q_s[b]	433.5	433.5	433.5	433.5	203.3	203.3	203.3	203.3
B_s	9.83	9.83	9.83	9.83	10.13	10.13	10.13	10.13
$-iN_Lh\nu^*_s$	19.75	7.27	5.32	4.44	16.55	5.86	4.24	3.51
Q_0	368.6	413.8	420.5	423.4	155.8	188.8	193.7	195.9
B_0	9.54	9.20	9.08	9.04	10.04	9.92	9.85	9.82
$-iN_Lh\nu^*_0$	19.46	7.03	5.11	4.26	16.48	5.80	4.18	3.46
Q_1	252.6	376.5	395.9	412.8	111.5	161.0	175.4	181.8
B_1	9.00	7.97	7.68	7.53	9.85	9.48	9.35	9.27
$-iN_Lh\nu^*_1$	18.89	6.54	4.70	3.89	16.33	5.67	4.08	3.36

[a] For notation see text. [b] All entries in kJ mol^{-1}.

ref 25 and 27. For reactions (R2)-(R4) a translational energy correction of +0.08 kJ mol^{-1} has been applied to account for the difference in the true asymptotic F_2 states and the actual value at the truncation point of the potential surface used in the quantum calculations; this correction remained unconsidered in ref 25 and 27 (for reaction (R1), the corresponding correction is negligibly small).

For reactions (R1) and (R2), the rotated Morse cubic spline fit may also deviate to some extent from the original surface in the vicinity of the barrier crest. In the mass scaled coordinate system used, the reactant's valley containing the barrier is very strongly compressed, and the standard mesh used in the spline interpolation is sufficiently wide in these cases to permit a deviation in the barrier height of about 0.15 kJ mol^{-1} for reaction (R1) and of about 0.10 kJ mol^{-1} for reaction (R2). Smaller ambiguities arise in the less compressed D and T cases.

The reference probabilities for reactions (R6) and (R7) were read off Figures 5, 7, 9, and 11 of ref 24.

Results from eq 6 and 7 using the VA parameters of Table II are compared with the quantum reaction probabilities in Figures 2-6. The results for the Bell parabola eq 7 are given separately only for the Mu and H reactions. For the other isotopes they do not deviate strongly from the Eckart permeabilities. Generally the agreement between the $P_v^E(E_T)$ and $P_v^Q(E_T)$ is excellent. There are slight deviations for reactions (R1) and (R2) which are in accordance with the observations about the potential fits noted above. An interesting additional deviation occurs for the light isotopes, Mu and H, at high translational energies, where the M1D probabilities are a little larger than the quantum ones. For D and T, agreement is perfect over the whole energy range. For these isotopes, the inverted parabola is also quite accurate with only slight deviations occurring at low energies. Predictably, the agreement of the Bell approach is not good in the muonium reactions, where the truncation error must become serious owing to the considerable reactivity in the vicinity of the energetic threshold. So, for Mu + F_2 (v = 0), the Bell formula predicts that $P_0^B(0)$ = 0.043, which will certainly lead to intolerably large errors in rate constant calculations at lower temperature.

A remarkable feature is the extremely good agreement of the Eckart approach with $P_1^Q(E_T)$ for all examples tested. This must mean that vibrational adiabaticity at the transition state is as well fulfilled for v = 1 as for v = 0. However, for Mu these barrier transmission probabilities may not be the final reaction probabilities. Both the quantum "line of no return" results and the barrier permeabilities may miss some back-reflection occurring later on the potential surface, namely, at the repulsive wall.[43]

In summary, reactions (R1)-(R8), and certainly other similar ones, can to an excellent approximation be understood in terms of one-dimensional barrier penetration, along the minimum energy path within a VA framework. Starting from extended LEPS surfaces, M1D effective potentials can be well enough approximated by an unsymmetric Eckart function, which permits a very convenient and simple treatment of these reactions. This state of affair differs somewhat from the one in H + H_2[4,18,19,21] owing to some particular properties of the

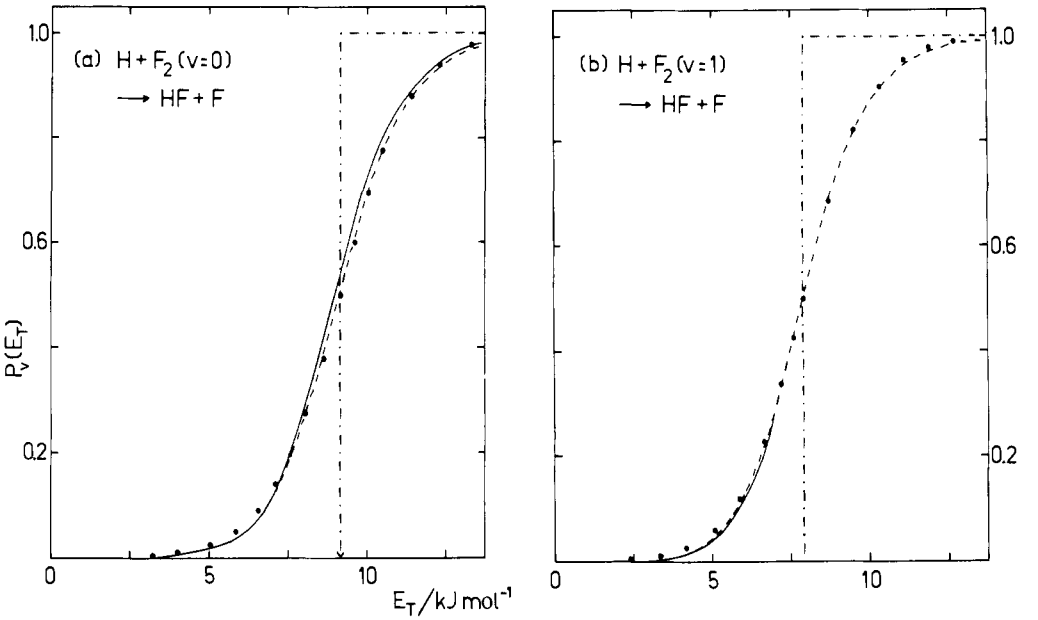

Figure 3. Comparison of quantum reaction probabilities and approximate ones for collinear H + F_2 (v). (a) v = 0. (b) v = 1. Full lines (—), quantum calculations;[25,27] dashed lines (- - -), VA Eckart; filled circles (●), VA Bell; dash-dotted (- · - ·), VA classical.

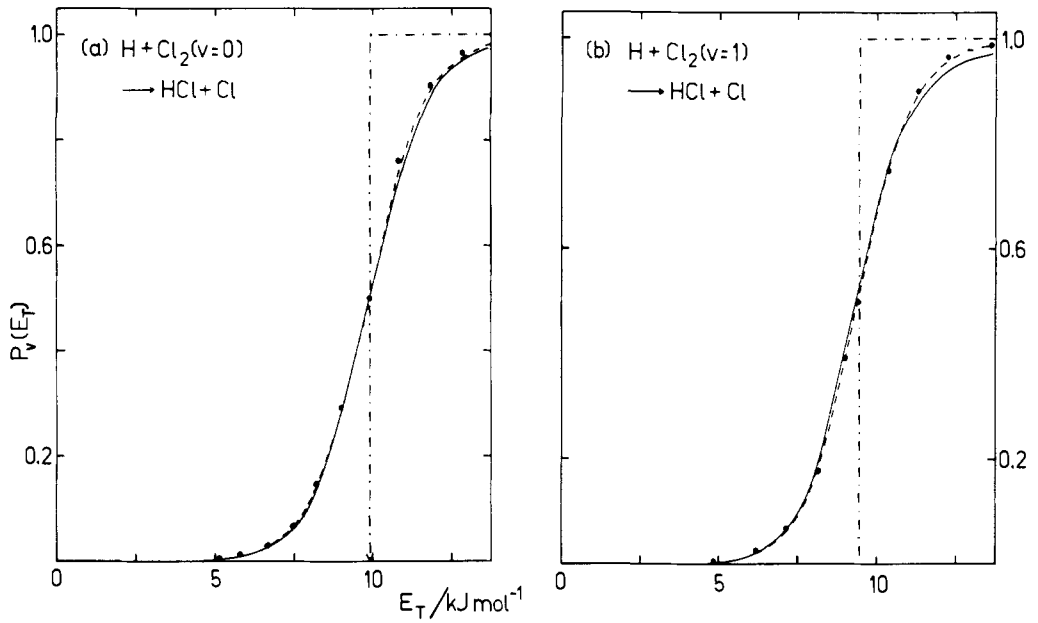

Figure 4. Comparison of quantum reaction probabilities and approximate ones for collinear H + Cl_2 (v). (a) v = 0. (b) v = 1. Full lines (—), quantum calculations;[24] dashed lines (- - -), VA Eckart; filled circles (●), VA Bell; dash-dotted (- · - ·), VA classical.

present reactions anticipated in the Introduction, namely, the absence of significant reaction path curvature in the barrier region and the rather low barrier height. Certainly at very low energies the Eckart function may well deviate from the "correct" effective potential, since only the shape of the barrier crest enters into eq 1. However, the extreme threshold range could not be tested, since there are no exact quantum results available in the range where $P_v^Q(E_T) \leq 0.001$.

In any case, these energy ranges do not contribute significantly to total reaction at temperatures above 200 K.

Returning again to the present results it is found that the CVE approximation does not give results in agreement with the quantum ones (this was also found for the H + H_2 reaction).[18,19] This can already be inferred from a superficial inspection of the quantum probabilities, which are indeed centered at the VA barrier heights, but not at the CVE values of 9.8 kJ mol^{-1} for X + F_2 or 10.1 kJ mol^{-1} for X + Cl_2. Contrary to the quantum results, the CVE results do not show a mass-dependent shift along the energy coordinate. Among the reactions treated here, the difference between the VA barrier height B_0 and the CVE value B_s is largest (0.79 kJ mol^{-1}) for reaction (R4); Figure 6 demonstrates clearly how the CVE results deviate from the quantum ones in this case.

Matters become still worse for vibrationally excited reactants, because the B_1 are even lower than the B_0 values. For reaction (R4), the difference between B_1 and B_s is already 2.30 kJ mol^{-1}. Generally for reactions (R1)-(R8), the use of the correct VA barrier height is more important than the use of the correct v^* values. This is manifested by the fact that the hybrid approach using (inconsistently) B_0 and v^*_s leads to results almost as good as the correct VA ones. This finding provides also an additional justification for the use of the scaling approximation, eq 5.

In Figures 2-6, step functions at the corresponding values

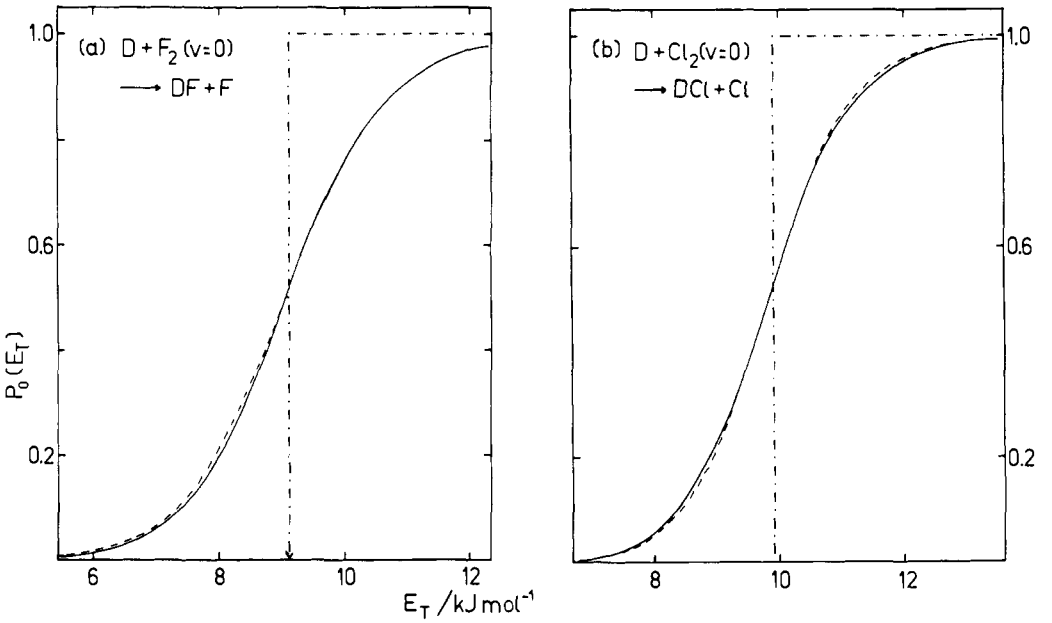

Figure 5. Comparison of quantum reaction probabilities and approximate ones for (a) collinear D + F_2 (v = 0); (b) collinear D + Cl_2 (v = 0). Full lines (—), quantum calculations;[24,27] dashed lines (- - -), VA Eckart; dash-dotted (- · -), VA classical.

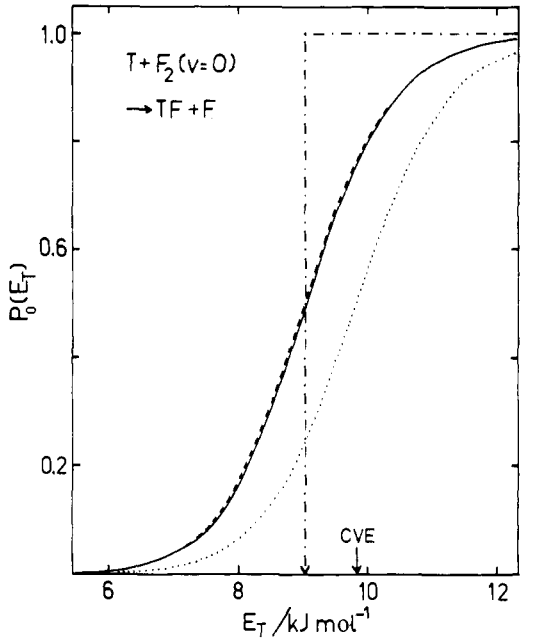

Figure 6. Comparison of quantum reaction probabilities and approximate ones for collinear T + F_2 (v = 0). Full line (—), quantum calculations;[27] dashed line (- - -), VA Eckart; dash-dotted (- · - ·), VA classical; dotted line (· · · ·), CVE Eckart. Arrow marked CVE indicates the CVE barrier height B_s.

of B_v are also shown. These are to be considered as the reference classical reaction probabilities, against which tunnelling is measured.

$$P_v^{CL}(E_T) = \begin{cases} 0 & E_T < B_v \\ 1 & E_T \geq B_v \end{cases} \tag{8}$$

These step functions are related to TST.[42] Alternatively, from a collisional point of view, they correspond to a one-dimensional analogue of (three-dimensional) hard sphere collisions with the critical energy of reaction being the one necessary to reach, adiabatically, the transition state.

Collinear classical trajectory calculations with fixed initial v have been carried out for reactions (R1)-(R4) and have been compared with the quantum results.[41] For reactions (R6) and (R7), Essen et al. considered a number of different techniques for collinear classical trajectories, and compared the corresponding results with each other and with exact quantum calculations.[24]

IV. Rate Constants and Activation Energies

From any of the various reaction probability curves given in section III, the corresponding rate constants for a fixed initial vibrational state and a Boltzmann distribution of translational energies corresponding to a temperature T can be calculated.[19,29,42]

$$k_v(T) = (2\pi\mu kT)^{-1/2} \int_0^\infty dE_T P_v(E_T) \exp(-E_T/RT) \tag{9}$$

(k is the Boltzmann constant and $R = N_L k$, the gas constant). The total thermal rate constants for fully Boltzmann distributed reactants can then be assembled from the weighted $k_v(T)$,[44]

$$k(T) = \sum_v \gamma_v k_v(T) \tag{10}$$

with $\gamma_v = \exp(-\epsilon_v/RT)/\Sigma_{v'} \exp(-\epsilon_{v'}/RT)$.

At 550 K, 98% of the F_2 molecules and 94% of the Cl_2 molecules are in v = 0 or 1, and it is sufficient to include two summation terms in (10) to obtain rate constants accurate to about 2%, provided that the missing 2 and 6% are treated as arising from v = 1 as well. For reactions (R2) and (R6), this has been checked by actually including higher terms. At higher temperatures, more than two terms should be included. In addition, at higher translational energies the reaction probabilities actually start to decrease again (see, e.g., the Mu + F_2 trajectory results[43] or the H + Cl_2 quantum results).[23,24] This behavior, however, is not reproduced by the $P_v^E(E_t)$ and $P_v^B(E_T)$ curves. In order to obtain the quantum rate constants $k_v^Q(T)$, the quantum reaction probability curves had to be extrapolated to high E_T values. A smooth graphical extrapolation governed by the Eckart results has been used. This of course does also not take into account a possible decrease of the $P_v^Q(E_T)$ at high energies. However, at lower temperatures neither this simplification nor the method of extrapolation has significant influence on the calculated rate constants, since the

Table III. Rate Constants, Tunnelling Correction Factors, and Isotopic Rate Constant Ratios at 300 K[a]

	Mu + F_2	H + F_2	D + F_2	T + F_2	Mu + Cl_2	H + Cl_2	D + Cl_2	T + Cl_2
k_0^{Q} [b]	1.47 (4)[c]	2.19 (3)	1.39 (3)	1.10 (3)		1.45 (3)	9.74 (2)	
k_0^{E}	1.61 (4)	2.13 (3)	1.40 (3)	1.12 (3)	1.14 (4)	1.47 (3)	9.71 (2)	7.77 (2)
Γ_0^{Q}	3.60	1.38	1.16	1.09		1.21	1.12	
Γ_0^{E}	3.94	1.34	1.17	1.11	3.42	1.24	1.12	1.08
Γ_0^{B}	5.30	1.42	1.20	1.13	4.40	1.27	1.13	1.08
Γ_0^{W}	(3.50)	1.33	1.18	1.12	(2.82)	1.23	1.12	1.08
f_0^{Q}	6.71	1	0.63	0.50		1	0.67	
f_0^{E}	7.57	1	0.66	0.53	7.72	1	0.65	0.52
f_0^{B}	9.57	1	0.64	0.50	9.72	1	0.64	0.51
f_0^{W}	(6.71)	1	0.67	0.53	(6.42)	1	0.66	0.53
f_0^{CL}	2.55	1	0.75	0.63	2.80	1	0.72	0.60
$(\mu_{X,Y_2}/\mu_{H,Y_2})^{-1/2}$	2.93	1	0.72	0.59	2.94	1	0.71	0.59
k_1^{Q}	1.85 (4)					1.75 (3)		
k_1^{E}	1.86 (4)	3.34 (3)	2.40 (3)	2.02 (3)	1.23 (4)	1.74 (3)	1.18 (3)	9.69 (2)
k^{E}	1.61 (4)	2.15 (3)	1.42 (3)	1.14 (3)	1.15 (4)	1.49 (3)	9.88 (2)	7.91 (2)
Γ_1^{E}	3.67	1.28	1.14	1.09	3.41	1.23	1.11	1.07
Γ^{E}	3.94	1.34	1.17	1.11	3.41	1.24	1.12	1.08

[a] For notation see text. [b] Rate constants in cm s^{-1} $molecule^{-1}$. [c] Numbers in parentheses indicate powers of 10.

Table IV. Rate Constants, Tunnelling Correction Factors, and Isotopic Rate Constant Ratios at 550 K[a]

	Mu + F_2	H + F_2	D + F_2	T + F_2	Mu + Cl_2	H + Cl_2	D + Cl_2	T + Cl_2
k_0^{Q} [b]	4.73 (4)[c]	1.28 (4)	8.83 (3)	7.23 (3)		1.03 (4)	7.32 (3)	
k_0^{E}	4.98 (4)	1.25 (4)	8.86 (3)	7.29 (3)	4.23 (4)	1.04 (4)	7.30 (3)	5.97 (3)
Γ_0^{Q}	1.52	1.12	1.05	1.03		1.06	1.05	
Γ_0^{E}	1.60	1.10	1.05	1.04	1.52	1.07	1.03	1.02
Γ_0^{B}	1.76	1.12	1.06	1.04	1.61	1.07	1.05	1.03
Γ_0^{W}	1.75	1.10	1.05	1.04	1.54	1.07	1.04	1.02
f_0^{Q}	3.69	1	0.69	0.56		1	0.71	
f_0^{E}	3.98	1	0.71	0.58	4.07	1	0.70	0.58
f_0^{B}	4.29	1	0.70	0.58	4.29	1	0.70	0.57
f_0^{W}	4.33	1	0.71	0.58	4.12	1	0.71	0.58
f_0^{CL}	2.72	1	0.74	0.61	2.86	1	0.72	0.60
$(\mu_{X,Y_2}/\mu_{H,Y_2})^{-1/2}$	2.93	1	0.72	0.59	2.94	1	0.71	0.59
k_1^{Q}	5.42 (4)					1.14 (4)		
k_1^{E}	5.50 (4)	1.62 (5)	1.19 (4)	1.01 (4)	4.43 (4)	1.15 (4)	8.14 (3)	6.74 (3)
k^{E}	5.05 (4)	1.30 (5)	9.23 (3)	7.63 (3)	4.28 (4)	1.07 (4)	7.58 (3)	6.16 (3)
Γ_1^{E}	1.57	1.08	1.05	1.03	1.52	1.07	1.03	1.02
Γ^{E}	1.60	1.09	1.05	1.04	1.52	1.07	1.03	1.02

[a] For notation see text. [b] Rate constants in cm s^{-1} $molecule^{-1}$. [c] Numbers in parentheses indicate powers of 10.

low-energy region dominates the rate constant integral. This was checked by using also different extrapolation schemes. At the other end of the energy scale, no quantum results are available in the threshold region, which will be of importance for low temperatures. For these reasons, the temperature interval from $T = 230$ K to $T = 900$ K has been considered in this work.

Among the reaction probability functions discussed in the previous section, only $P_v^{CL}(E_T)$ can be integrated analytically to yield the well-known form

$$k_v^{CL}(T) = (kT/2\pi\mu)^{1/2} \exp(-B_v/RT) \qquad (11)$$

The quantum, Eckart, and Bell rate constants k_v^{Q}, k_v^{E}, and k_v^{B} have to be obtained from numerical integration of eq 17, inserting P_v^{Q}, P_v^{E}, and P_v^{B}, respectively.

The calculated rate constants $k_0^{Q}(T)$ and $k_0^{E}(T)$ for (R1)–(R8), $T = 300$ and 550 K, are displayed in Tables III and IV. Classical rate constants and the Bell ones can be calculated from the tunnelling correction factors $\Gamma_0(T)$ also given.

$P_v^{E}(E_T)$ and $P_v^{B}(E_T)$ differ from $P_v^{CL}(E_T)$ solely due to nonclassical potential barrier transmission, and the same is then true for the rate constants. The tunnelling correction factor to the classical rate constant is therefore[12,19,32]

$$\Gamma_v^{E}(T) = k_1^{E}(T)/k_v^{CL}(T) \qquad (12a)$$

$$\Gamma_v^{B}(T) = k_v^{B}(T)/k_v^{CL}(T) \qquad (12b)$$

The quotient

$$\Gamma_v^{Q}(T) = k_v^{Q}(T)/k_v^{CL}(T) \qquad (12c)$$

will in principle also contain all contributions arising from the neglect of one mathematical dimension. However, for the present reactions, no such contributions are of importance, and it is apt to call $\Gamma^{Q}(T)$ a tunnelling correction factor as well.

Wigner's tunnelling correction factor $\Gamma^{W}(T)$ is also included in the tables. This is valid for small amounts of tunnelling and is[45]

$$\Gamma^{W}(T) = 1 + \frac{1}{24}\left|h\nu^*/kT\right|^2 \qquad (13)$$

The numerical values given are derived using ν_0^*, keeping to the spirit of the VA method. Note, however, that Wigner's original application of his tunnelling correction factor employed ν_s^*.[45]

As can be seen from the results, and as expected from the behavior of the reaction probabilities, $k_v^{E}(T)$ is usually very close to $k_v^{Q}(T)$, except for the small deviation for reaction (R1) which is probably due to the potential surface fit. The Bell

Table V. Tolman Activation Energies at 300 and 550 K[a]

		Mu + F_2	H + F_2	D + F_2	T + F_2	Mu + Cl_2	H + Cl_2	D + Cl_2	T + Cl_2
$E_{A,0}^{Q}$	300 K	5.3	9.0	9.5	9.8		10.1	10.5	
$E_{A,0}^{E}$		4.9	9.0	9.5	9.7	5.9	10.1	10.5	10.7
$E_{A,0}^{B}$		3.7	8.6	9.4	9.6	4.6	9.9	10.5	10.7
$E_{A,0}^{W}$		(7.2)	9.2	9.6	9.7	(8.1)	10.3	10.6	10.7
$E_{A,0}^{CL}$		10.8	10.5	10.3	10.3	11.3	11.2	11.1	11.1
$E_{A,1}^{Q}$		4.9					9.8		
$E_{A,1}^{E}$		4.7	8.0	8.2	8.3	5.7	9.7	10.1	10.2
E_{A}^{E}		4.9	9.0	9.5	9.7	5.9	10.1	10.5	10.7
$E_{A,0}^{Q}$	550 K	8.1	10.6	11.0	11.1		11.7	11.8	
$E_{A,0}^{E}$		7.9	10.7	10.9	11.0	8.9	11.6	11.8	11.9
$E_{A,0}^{B}$		7.0	10.6	10.9	11.0	8.2	11.6	11.8	11.9
$E_{A,0}^{W}$		7.9	10.7	10.9	11.0	9.1	11.6	11.8	11.9
$E_{A,0}^{CL}$		11.8	11.5	11.4	11.3	12.3	12.2	12.1	12.1
$E_{A,1}^{Q}$		7.6					11.2		
$E_{A,1}^{E}$		7.6	9.6	9.6	9.6	8.7	11.2	11.4	11.4
E_{A}^{E}		7.8	10.6	10.8	10.8	8.8	11.5	11.7	11.8

[a] All entries in kJ mol^{-1}.

approach need not be discussed further; at low temperatures $\Gamma_v^{B}(T)$ is always too large and should not be used. The Wigner correction, which neglects higher orders of $|h\nu^*/kT|^2$, should not be applied if $|h\nu^*| \gg kT$, as is the case for the Mu reactions at 300 K. Notwithstanding this fact, the $\Gamma_0^{W}(T)$ turn out to be a good first-guess-type approximation to the quantum results even in these cases. For the heavier isotopes H, D, and T, agreement with quantum results is extremely good, and $\Gamma_0^{W}(T)k_0^{CL}(T)$ may serve as a very good analytic expression for $k(T)$.

The isotopic rate constant ratios (relative rate constants), $f_{(X)}(T) = k_{(X)}(T)/k_{(H)}(T)$, contain a factor $(\mu_{H,Y_2}/\mu_{X,Y_2})^{1/2}$, with Y = F, Cl (which for the mass combinations studied here is close to $(\mu_H/\mu_X)^{1/2}$). This is also the high-temperature limit for all of the various rate constants; in the present examples the k (900) are already close to this behavior. At lower temperatures, only the classical rate constant ratios are close to this value, with deviations coming from the mass-dependent and hence differing values of B_v in $\exp(-B_v/RT)$. For the nonclassical rate constant ratios deviations due to the different amount of tunnelling for the different isotopes become considerable at room temperature, in particular for the muonium reactions. This illustrates the exciting possibilities opened by introducing experimental muonium chemistry,[46-48] with respect to exploring tunnelling, or to discriminating between theoretical models or potential surfaces. In Tables III and IV, rate constants, tunnelling corrections, activation energies, and isotopic rate constant ratios for reaction out of $v = 1$, as well as those for a Boltzmann ensemble of vibrational levels, are also included for the Eckart approach. Their relation to the corresponding values from the other approaches resembles the situation for $v = 0$. One can also arrive at the thermal rate constants $k^{E}(T)$ derived above via simple classical TST plus Eckart corrections,[3]

$$k^{TST/E}(T) = \Gamma^{E}(T)(kT/2\pi\mu)^{1/2}\frac{Q^{\ddagger}_{v}}{Q^{0}_{v}}\exp(-B/RT) \quad (14)$$

with $Q^{\ddagger}_{v}$ and Q^{0}_{v} being vibrational partition functions of the transition state and the reactant molecule, respectively. The tunnelling correction factor $\Gamma^{E}(T)$ is an average over the $\Gamma_v^{E}(T)$ given above, using the $k_v^{CL}(T)$ as weights. Thus Eckart-corrected classical TST is extremely accurate for the reactions considered (at least in the temperature interval 230-900 K). Care has only to be given to selecting the correct VA barrier height and width. The last point may be illustrated by considering the CVE rate constants. With the ν_s^* values being similar to the VA ones, CVE rate constants will differ from the VA ones mainly by a factor $\exp\{(B_v - B_s)/RT\}$. At

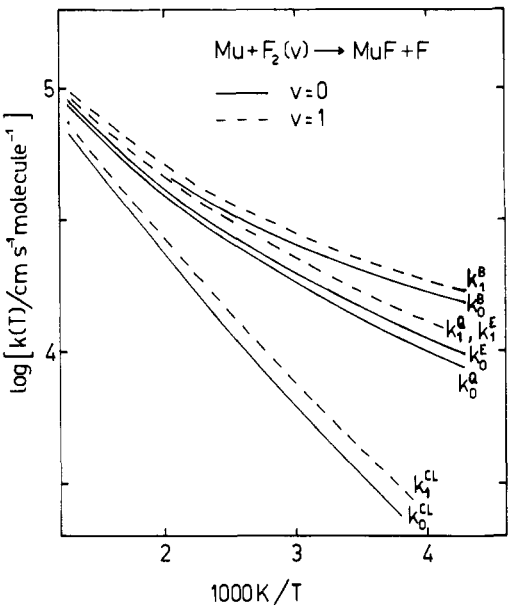

Figure 7. Arrhenius plots for collinear Mu + F_2 (v). Full lines (—), v = 0; dashed lines (- - -), v = 1. Results shown are exact quantum (Q), VA Eckart (E), VA Bell (B), and VA classical (CL). k_1^{Q} and k_1^{E} coincide over the whole range.

300 K, this amounts to errors of ≈11% for Mu + F_2 ($v = 0$), ≈27% for T + F_2 ($v = 0$), and ≈60% for T + F_2 ($v = 1$). Clearly, the CVE approximation cannot be used for the present family of reactions.

Finally, Tolman activation energies[49] are presented in Table V. These are given by the local slope of the Arrhenius plot, that is,[50,51]

$$E_A(T) = -\left.\frac{\partial \ln k(T')}{\partial(1/RT')}\right|_T \quad (15)$$

From eq 11, the classical activation energy in VA approximation is

$$E_{A,v}^{CL}(T) = B_v + \tfrac{1}{2}RT \quad (16)$$

The activation energy for Wigner corrected rate constants is

$$E_{A,v}^{W}(T) = B_v + \tfrac{1}{2}RT - \frac{N_L^2|h\nu_v^*|^2}{12\Gamma_v^{W}(T)RT} \quad (17)$$

Activation energies for the other approaches must be obtained numerically by inserting eq 9 into eq 15. The accuracy of the approximate values follows the same pattern as for the rate

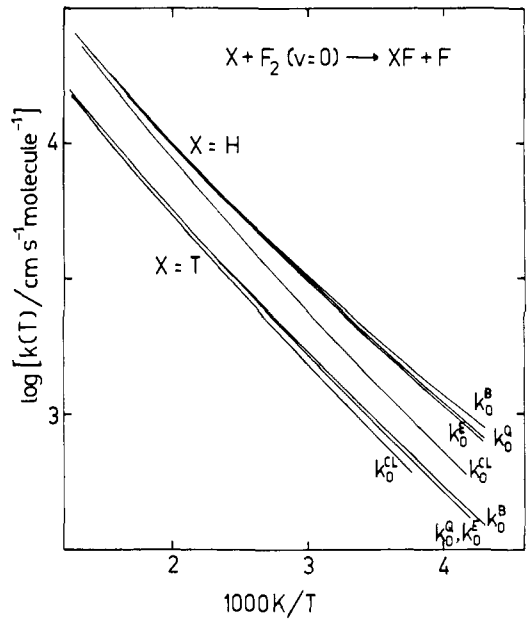

Figure 8. Arrhenius plots for collinear H + F_2 (v = 0) and T + F_2 (v = 0). Results shown are exact quantum (Q), VA Eckart (E), VA Bell (B), and VA classical (CL). k_0^Q and k_0^E coincide over the whole range.

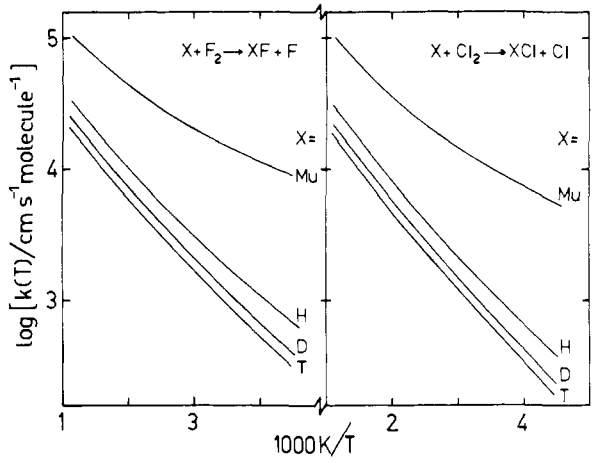

Figure 9. Arrhenius plots for collinear X + F_2 and X + Cl_2, for Boltzmann distributed reactants. Plots shown are for $k^E(T)$.

constants. Again, the simple Wigner approach leads to very good agreement with quantum mechanical results except for the Mu reaction at 300 K (and below).

For some of the reactions where quantum results are available, Arrhenius plots for $k_c(T)$ are shown in Figures 7 and 8. For reactions (R2) and (R4), $k_0^Q(T)$ and $k_0^E(T)$ are seen to coincide over the whole temperature range (at the scale of the figure). Reactions (R3), (R6), and (R7) are not shown separately. Again $k_0^Q(T)$, $k_0^E(T)$ (and $k_0^B(T)$) would coincide. Owing to the term $T^{1/2}$ in eq 11, the classical Arrhenius plots are weakly curved. Tunnelling contributions cause an increase in this curvature at lower energies. In particular, Arrhenius plot curvature is considerable for reaction (1). Again the good agreement between the quantum rates and the Eckart approximation is evident.

Figure 9 shows the isotope dependence of the Arrhenius plots, using Eckart-thermal rate constants $k^E(T)$. The decrease of the rate constants, and the decreasing influence of tunnelling on going from Mu to T, is nicely illustrated. However, it is evident that even for the strong tunnelling case Mu + F_2 deviations from linearity are not terribly prominent over restricted temperature ranges such as usually covered experimentally. Extrapolating to three dimensions, this means that unambiguous experimental detection of Arrhenius curvature would probably require a temperature interval extending over the major part of the one plotted in Figure 9.

Part of the material in this section parallels investigations of Truhlar et al.,[52,53] although for the most part the present paper is complementing ref 52. Truhlar et al. have determined quantum, classical, and Wigner corrected rate constants for reaction (R6). In particular, they have focused on comparison with classical trajectory rate constants. Classical trajectory and exact quantum rate constants have also been compared by Essen et al.[24] for reactions (R6) and (R7), and by Connor et al.[41] for reactions (R1)-(R4).

V. Conclusions

Starting initially from extended LEPS potential surfaces, the VA approximation is found entirely adequate to describe accurately reaction probabilities and rate constants (at least in the range 230-900 K) of the collinear reactions (R1)-(R8). Furthermore, it is sufficient to use an Eckart fit to the M1D potential describing reaction path motion, and to use a scaling relation to obtain the tunnelling frequencies for these effective potentials. Since the agreement extends over a considerable range of translational energies, it is not likely to be brought about by fortuitous cancellation of errors. Hence each of the approximation assumptions involved should actually be closely fulfilled (that is, vibrational adiabaticity assumptions, separability, neglect of reaction path curvature, asymmetric Eckart-like shape of the M1D potential, and so on).

This offers a fast, convenient, and economic method of computing collinear reaction probabilities and kinetic data for reactions such as (R1)-(R8), particularly if scanning over a large number of potential surfaces is involved, e.g., in investigations of the potential surface dependence of reactions. An extension of the investigations to the three-dimensional case is attempted in another paper.[40]

Acknowledgments. The numerical calculations reported were carried out on the CDC Cyber 73 at the Computer Centre of Vienna University. The allocation of computer time is gratefully acknowledged. I am grateful to Drs. H. Lischka and A. Karpfen for providing me with their programs for normal mode analysis, and to Drs. J. Manz and J. N. L. Connor for reading the manuscript.

References and Notes

(1) D. L. Bunker, "Theory of Elementary Gas Reactions", Pergamon Press, Oxford, 1966.
(2) H. S. Johnston, "Gas Reaction Rate Theory", Ronald Press, New York, N.Y., 1966.
(3) D. G. Truhlar and A. Kuppermann, *J. Am. Chem. Soc.*, **93**, 1840 (1971).
(4) D. G. Truhlar and R. E. Wyatt, *Annu. Rev. Phys. Chem.*, **27**, 1 (1976).
(5) C. Eckart, *Phys. Rev.*, **35**, 1303 (1930).
(6) R. P. Bell, *Proc. R. Soc. London, Ser. A*, **148**, 241 (1935).
(7) R. P. Bell, *Trans Faraday Soc.*, **55**, 1 (1959).
(8) E. F. Caldin, *Chem. Rev.*, **69**, 135 (1969).
(9) S. Glasstone, K. J. Laidler, and H. Eyring, "The Theory of Rate Processes", McGraw-Hill, New York, N.Y., 1941.
(10) R. E. Weston, Jr., and H. A. Schwarz, "Chemical Kinetics", Prentice-Hall, Englewood Cliffs, N.J., 1972.
(11) D. G. Truhlar and A. Kuppermann, *Chem. Phys. Lett.*, **9**, 269 (1971).
(12) H. S. Johnston, *Adv. Chem. Phys.*, **3**, 131 (1960).
(13) H. S. Johnston and D. Rapp, *J. Am. Chem. Soc.*, **83**, 1 (1961).
(14) R. A. Marcus, *J. Chem. Phys.*, **49**, 2617 (1968).
(15) R. E. Wyatt, *J. Chem. Phys.*, **51**, 3489 (1969).
(16) R. A. Marcus, *J. Chem. Phys.*, **45**, 4493 (1966).
(17) R. A. Marcus, *J. Chem. Phys.*, **46**, 959 (1967).
(18) D. G. Truhlar and A. Kuppermann, *J. Chem. Phys.*, **52**, 3841 (1970).
(19) D. G. Truhlar and A. Kuppermann, *J. Chem. Phys.*, **56**, 2232 (1972).
(20) R. A. Marcus and M. E. Coltrin, *J. Chem. Phys.*, **67**, 2609 (1977).
(21) E. M. Mortensen, *J. Chem. Phys.*, **48**, 4029 (1968).
(22) R. J. LeRoy, K. A. Quickert, and D. J. LeRoy, *Trans. Faraday Soc.*, **66**, 2997 (1970).
(23) M. Baer, *J. Chem. Phys.*, **60**, 1057 (1974).
(24) H. Essen, G. D. Billing, and M. Baer, *Chem. Phys.*, **17**, 443 (1976).
(25) J. N. L. Connor, W. Jakubetz, and J. Manz, *Chem. Phys. Lett.*, **39**, 75 (1976).

(26) J. N. L. Connor, W. Jakubetz, and J. Manz, *Chem. Phys. Lett.*, **45**, 265 (1977).
(27) J. N. L. Connor, W. Jakubetz, and J. Manz, *Chem. Phys.*, **28**, 219 (1978).
(28) K. Morokuma and M. Karplus, *J. Chem. Phys.*, **55**, 63 (1971).
(29) M. A. Eliason and J. O. Hirschfelder, *J. Chem. Phys.*, **30**, 1426 (1959).
(30) D. G. Truhlar, *J. Chem. Phys.*, **53**, 2041 (1970).
(31) J. M. Bowman, A. Kuppermann, J. T. Adams, and D. G. Truhlar, *Chem. Phys. Lett.*, **20**, 229 (1973).
(32) I. Shavitt, *J. Chem. Phys.*, **31**, 1359 (1959).
(33) P. J. Kuntz in "Modern Theoretical Chemistry", Vol. II, "Dynamics of Molecular Collisions", Part B, W. H. Miller, Ed., Plenum Press, New York, N.Y., 1976, p 53.
(34) N. Jonathan, S. Okuda, and D. Timlin, *Mol. Phys.*, **24**, 1143 (1972).
(35) P. J. Kuntz, E. M. Nemeth, S. D. Rosner, J. C. Polanyi, and C. E. Young, *J. Chem. Phys.*, **44**, 1168 (1966).
(36) J. C. Polanyi, J. L. Schreiber, and J. J. Sloan, *Chem. Phys.*, **9**, 403 (1975).
(37) H. S. Johnston and J. Heicklen, *J. Phys. Chem.*, **66**, 532 (1962).
(38) E. B. Wilson, J. C. Decius, and P. Cross, "Molecular Vibrations", McGraw-Hill, New York, N.Y., 1955.
(39) R. A. Marcus, *J. Chem. Phys.*, **41**, 610 (1964).
(40) W. Jakubetz, in preparation.
(41) (a) J. N. L. Connor, W. Jakubetz, and A. Laganà, *J. Phys. Chem.*, in press; (b) Abstracts, Symposium on Current Status of Kinetics of Elementary Gas Reactions, F. Kaufman, Ed., NBS, Gaithersburg, 1978, p 45.
(42) K. Morokuma, B. C. Eu, and M. Karplus, *J. Chem. Phys.*, **51**, 5193 (1969).
(43) J. N. L. Connor and A. Laganà, to be published.
(44) B. Widom, *Science*, **148**, 1555 (1965).
(45) E. Wigner, *Z. Phys. Chem., Abt. B*, **19**, 203 (1932).
(46) D. G. Fleming, D. M. Garner, J. H. Brewer, J. B. Warren, G. M. Marshall, G. Clark, A. E. Pifer, and T. Brown, *Chem. Phys. Lett.*, **48**, 393 (1977).
(47) D. G. Fleming, J. H. Brewer, and D. M. Garner, *Ber. Bunsenges. Phys. Chem.*, **81**, 159 (1977).
(48) D. M. Garner, D. G. Fleming, and J. H. Brewer, *Chem. Phys. Lett.*, **55**, 163 (1978).
(49) R. C. Tolman, *J. Am. Chem. Soc.*, **42**, 2506 (1920).
(50) M. Karplus, R. N. Porter, and R. D. Sharma, *J. Chem. Phys.*, **43**, 3259 (1965).
(51) M. Menzinger and R. L. Wolfgang, *Angew. Chem.*, **81**, 446 (1969).
(52) D. G. Truhlar, J. A. Merrick, and J. W. Duff, *J. Am. Chem. Soc.*, **98**, 6771 (1976).
(53) (a) D. G. Truhlar, *J. Phys. Chem.*, in press; (b) ref 41b, p 84.

Sudden Polarization: Pyramidalization of Twisted Ethylene

Bernard R. Brooks and Henry F. Schaefer III*

Contribution from the Department of Chemistry, University of California, Berkeley, California 94720. *Received May 29, 1978*

Abstract: Nonempirical molecular electronic structure theory has been used to investigate the concept of "sudden polarization". In particular, the departure of twisted ethylene from ideal D_{2d} geometries has been studied. Initially, configuration interaction (CI) studies of all four electronic states (of twisted C_2H_4) arising from the e^2 orbital occupancy were completed. The predicted C-C bond distances and energies relative to the planar ground state follow: $^1B_1$ (N state) 1.49 Å, 2.6 eV; $^3A_2$ (T state) 1.49 Å, 2.7 eV; $^1B_2$ (V state) 1.40 Å, 5.9 eV; $^1A_1$ (Z state) 1.40 Å, 5.8 eV. A major theoretical problem for the zwitterionic Z and V states is to formulate a type of wave function which passes smoothly and correctly from D_{2d} to non-D_{2d} geometries. This problem has been solved and the ensuing calculations predict rather large dipole moments as the Z and V states become pyramidalized. For example, with one of the CH_2 groups bent out of its D_{2d} plane by only 5°, the Z and V state dipole moments μ_z (along the C-C axis) are +1.25 and −1.18 D, respectively. The differing dipole moment signs are meant to imply that for the Z state, the pyramidalized methylene carries the negative charge. The Z state, the lower of the two zwitterionic states, has a pyramidalization angle θ of 31° at its equilibrium geometry.

Background and Development

Although the planar ground state of ethylene is stable with respect to the twisting of the double bond, this is not true of the low-lying states. At the perpendicular D_{2d} ($\theta = 90°$) geometry there are four π^2 ($2e^2$) states.[1,2] The two lowest of these states, which are quite close in energy, are the $^1B_1$ (N state) and the $^3A_2$ (T state). The highest two, also quite close to each other in energy, are the $^1B_2$ (V state) and the $^1A_1$ (Z state). Only the lowest of the four states (N state), which correlates with the planar ground state and corresponds to the rotational barrier of ethylene, is unstable with respect to twisting from the D_{2d} geometry. The other low-lying twisted state ($^3A_2$ state) correlates with the planar $^3B_{1u}$ (π,π^*) T state.

The higher pair are known to be ionic[1,3] and highly polarizable[4] and thus are considered to be zwitterionic states. Of these, the $^1B_2$ or V state correlates with the planar $^1B_{1u}$ (π,π^*) V state while the $^1A_1$ or Z state correlates with a much higher planar state where both π electrons have been excited to the π^* orbital. In the absence of an external field, in D_{2d} symmetry, the wave functions of the zwitterionic states may be qualitatively described as

$$\text{Z state} \quad \psi = \phi_A(1)\phi_A(2) + \phi_B(1)\phi_B(2) \qquad (1)$$

$$\text{V state} \quad \psi = \phi_A(1)\phi_A(2) - \phi_B(1)\phi_B(2) \qquad (2)$$

where the atomic carbon p orbitals ϕ_A and ϕ_B are sketched below.

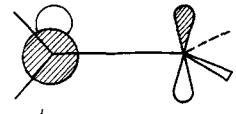

ϕ_A ϕ_B

As written neither of these states has a dipole moment. However, when an interaction is introduced by an external field or by a geometry change these states may mix, causing distinct polarity. The requirements for mixing are that first, there must be little or no incipient overlap between radical sites, and second, that there must be a dissymmetry between the sites.[5] In other related systems of interest, substituents other than hydrogen may also result in the necessary dissymmetry between the radical sites.

Bonacic-Koutecky, Bruckmann, Hiberty, Koutecky, Leforestier, and Salem have noted[5] that the charge separation for the related allyl system peaks very sharply about the twisted geometry and drops to practically zero outside a narrow 2° region about $\theta = 90°$. This is the origin of the term "sudden polarization". This zwitterionic polarization can be qualitatively understood by the coupling matrix

$$H = \begin{pmatrix} E_a - E & H_{ab} \\ H_{ab} & E_b - E \end{pmatrix} \qquad (3)$$

where E_a and E_b are the electronic energies of the ionic forms of ϕ_A and ϕ_B, and H_{ab} represents the exchange and overlap terms between the two forms.

0002-7863/79/1501-0307$01.00/0